JOURNAL OF AIRCRAFT
Vol. 30, No. 5, Sept.–Oct. 1993

Unsteady Subsonic Aerodynamics for Bodies and Wings with External Stores Including Wake Effect

P. C. Chen*
ZONA Technology, Inc., Mesa, Arizona 85210
and
H. W. Lee† and D. D. Liu‡
Arizona State University, Tempe, Arizona 85287

An unsteady subsonic method has been developed for aerodynamic computations of any elastic or rigid aircraft with external stores. The method consists of two integral parts: 1) a body surface panel method (SPM), and 2) a constant-pressure lifting surface method, which is the subsonic parallel of the harmonic gradient method (HGM) (or the ZONA51 code) for unsteady supersonics. The body considered can be flat-based or close-ended and its geometry input is amenable to any given fuselage or store configuration. The present method is considered an advancement over the past development at least in three aspects: 1) correct unsteady boundary condition on body, 2) a new wake model to account for the body/wake effect, and 3) improved accuracy in wing-body interference. Various AGARD lifting surfaces, truncated blunt and pointed bodies, and a number of NLR wing-store-tiptank combinations were studied for method validation. The present method has shown substantial improvement in the pressures, stability derivatives, and airloads on these configurations. For all cases considered, the present results, with or without the wake model, have consistently shown closest agreement with all measured data among existing methods. Therefore, we believe that an accurate and effective method is finally at hand for subsonic aeroelastic applications.

Nomenclature

A	=	panel area
C_{p_0}, C_p	=	steady and unsteady pressure coefficients
h_B	=	(h_B, h'_B, h''_B) body structure mode, its slope and curvature
h_W	=	wing structural mode parallel to the outward normal vector
k	=	reduced frequency
L	=	physical body length
M	=	freestream Mach number
$\boldsymbol{n}$	=	(n_x, n_y, n_z) unit outward normal vector of each panel
V_B	=	$\nabla\phi_B$, perturbed unsteady velocity vector on the body
V_W	=	$\nabla\phi_W$, perturbed unsteady velocity vector on the wing
V_0	=	$\nabla\phi_0$, perturbed steady velocity vector
x_0, y_0, z_0	=	location of the control point
$\bar{x}_0$ or X_G	=	pitching axis location
β	=	$(1 - M^2)^{1/2}$
δ_0	=	small amplitude of oscillation
μ	=	unknown doublet strength
ν	=	kM/β
(ξ, η, ζ)	=	$(x_0 - x, y_0 - y, z_0 - z)$
σ	=	unknown source strength
τ	=	body thickness ratio
ϕ_0, ϕ	=	perturbed steady and unsteady velocity potentials

Subscripts

$(\cdot)_i$	=	$(\cdot)$ of the ith panel
$(\cdot)_j$	=	$(\cdot)$ of the jth panel

Superscripts

$(\cdot)^{(I)}$	=	$(\cdot)$ of the Ith structural mode
$(\cdot)^{(J)}$	=	$(\cdot)$ of the Jth structural mode

Introduction

THE problem of the wing-store interactions for fighter aircraft during its subsonic flight phase has been a major concern for aircraft performance, design, and analysis. The doublet lattice method (DLM) for lifting surfaces[1] and for wing-bodies[2] has been widely adopted as unsteady aerodynamic tools for subsonic aeroelastic applications. In Ref. 2, improved DLM has been effective in treatments of bodies of revolution that is sufficiently slender and could receive moderate lifting contributions due to flowfield asymmetry. The consistent formulation of Morino's method[3] using the combination of source and doublet panels to solve the wing-body aerodynamics, has opened ways for subsequent development of steady panel codes, e.g., Refs. 4–6. Although Marino's approach generally includes unsteady flow formulation, it has generated limited computed results which prevents one from assessing its validity for application.

A more comprehensive unsteady wing-body method has been developed by NLR during the mid-70s[7,8] and was recently further documented in Ref. 9. The NLR method employs the DLM and a constant-source panel method to represent wings and bodies, respectively. Numerical study was performed to validate the computed results with the NLR test data exclusively for the NLR's wing with pylon and stores model.[8,10] Presumably, the NLR approach is based on the wind-fixed system that was formulated by Labrijere and Sytsma[11] and that of Ref. 7. It is our opinion that the apex singularity issue results from this system have not been properly clarified. Furthermore, the lifting-surface representation of the body wake used in Ref. 8 is physically unrealistic.

Received Aug. 16, 1991; revision received June 2, 1992; accepted for publication June 2, 1992.

*President. Member AIAA.
†Research Assistant, Mechanical and Aerospace Engineering; currently Lt. Colonel, Korean Air Force.
‡Professor, Mechanical and Aerospace Engineering. Member AIAA.

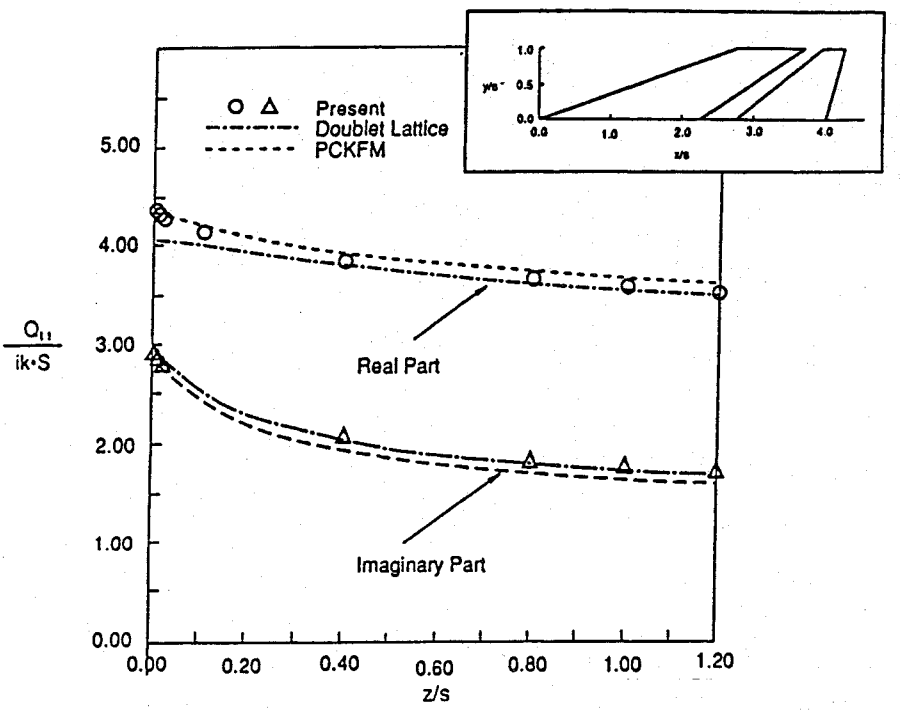

Fig. 1 Variation of lift coefficients of the nonplanar AGARD wing-tail configuration with heave mode vs tail height; $M = 0.8$ and $k = 1.5$.

It appears that little has been advanced in the topic area since NLR group first published their results some 15 yr ago. Also, all previous works have provided insufficient information regarding independent verification of the body-alone aerodynamics, which, in our opinion, should be taken as an essential step in the development of unsteady wing-body aerodynamics for aeroelastic analysis.

As a counterpart of our unsteady supersonic method development for lifting surfaces and wing-body (HGM/ZONA51 code and ZONA7 code series), our recent unsteady subsonic development is considered an advancement over the previous methods in the following issues: 1) correct unsteady boundary condition is applied on the body surface; 2) body/wake effect due to flow separation at the body base is properly accounted for by introducing a new imbedded-singularity wake model; and 3) wing-body influence can be more accurately accounted for as a result of that our lifting surface method adopts the constant pressure panel approach, as opposed to the DLM approach.

Therefore, the objective of this article is twofold. First, with these improved issues, a new approach to the computation of unsteady subsonic flow for wing-body will be presented. Second, numerous cases studied, including various lifting surface, bodies, and several cases of wing with external stores, are conducted for the purpose of method validation.

Approach

The present approach adopts the similar paneling scheme to that of our unsteady supersonic wing-body method[12] (i.e., the ZONA7 code). The bodies adopt the constant-source paneling, whereas, the wing planforms adopt the constant-pressure paneling.

Kernel Formulation

First, the body surfaces are divided in number of body panels (NB), whereas, the lifting surfaces by number of wing panels (NW) (see Fig. 1). For an ith control point located at (x_0, y_0, z_0) on the wing or body panels, the unsteady perturbed potential represented by ϕ can be discretized as

$$\phi_i(x_0, y_0, z_0) = \sum_{j=1}^{NB} \phi_{B_{ij}} \sigma_j + \sum_{j=1}^{NW} \phi_{W_{ij}} \Delta C_{pj} \tag{1}$$

where σ_j is the unknown constant source strength on the jth body panel, and ΔC_{pj} is the unknown pressure jump on the jth wing panel.

The discretized $\phi_{B_{ij}}$ and $\phi_{W_{ij}}$ represent the potential influence coefficient (PIC) indicating a unit potential change of the jth panel of the body and wing, respectively, to the ith control point; they are

$$\phi_{W_{ij}} = \frac{\beta}{8\pi} I_{W_{ij}}[e^{-ik\beta\xi} K_j]$$

where

$$I_{W_{ij}}[\cdot] \equiv \int_{\Delta\eta_j} \int_{\Delta\xi_j} [\cdot]\, d\xi\, d\eta \tag{2}$$

$$\phi_{B_{ij}} = -\frac{1}{4\pi} I_{B_{ij}}[e^{-ivM\xi} H_j]$$

where

$$I_{B_{ij}}[\cdot] \equiv \int_{\Delta\xi_j} \int_{\Delta\eta_j} [\cdot]\, d\eta\, d\xi \tag{3}$$

and $k = \omega L/U_\infty$ is the reduced frequency, ω is the circular frequency due to oscillatory motion, U_∞ is the freestream speed, and L is the characteristic length.

The kernels associated with the above integrals reads

$$K_i = \frac{\partial}{\partial n} \int_{-\infty}^{\xi} \frac{\exp[ik(\lambda - M\sqrt{\lambda^2 + r^2})]/\beta}{\sqrt{\lambda^2 + r^2}}\, d\lambda \tag{4}$$

$$H_i = (e^{-ivR_i}/R_i) \tag{5}$$

For convenience, we drop the subscripts i and j for this point onward. Thus, the terms on the right side of Eqs. (4) and (5) are interpreted as

$$R = (\xi^2 + r^2)^{1/2}$$

$$r^2 = \eta^2 + \zeta^2$$

$\Delta\eta$ and $\Delta\xi$ define the boundaries of the jth panel, and $\partial/\partial n$ denotes the differentiation with respect to the normal of the wing panel.

To evaluate the integral Eq. (4), Lashka's exponential substitution procedure[13] is applied. Here, only 11 terms in Desmaris' series D24.2[14] are used and found adequate for satisfactory accuracy.

Next, the velocity influence coefficients (VIC) can be derived by taking the spatial gradients of Eqs. (2) and (3) for wing and body respectively, i.e.

$$V_W = (\beta/8\pi)\, I_{W_{ij}}[\nabla(e^{-ik\beta\xi}K)] \qquad V_W = (u_{W_{ij}}, v_{W_{ij}}, w_{W_{ij}}) \tag{6}$$

$$V_B = [-(1/4\pi)]I_{B_{ij}}[\nabla(e^{-i\nu M\xi}H)] \qquad V_B = (u_{B_{ij}}, v_{B_{ij}}, w_{B_{ij}}) \tag{7}$$

Computations of Eqs. (2), (3), (6), and (7) requires special treatments in their numerical integration schemes. Care must be taken in the regions where these integrals become singular (e.g., see Ref. 15). Moreover, it will be seen that to handle these integrals for wings is different from that for the body.

Numerical Integration Scheme

For wing panels, chordwise integration is performed first for Eqs. (2) and (6). As no singular integral occurs here, standard schemes such as Gaussian Quadrature can be employed for numerical evaluations. However, for spanwise integration, the integrands of Eqs. (2) and (6) become singular in the self-influencing strip for both the planar and coplanar cases. In such a case, a special integration scheme was developed, similar to the technique used in the DLM, to resolve the singular integrals. For the control point located outside of the self-influencing strip the integrands are regular, and consequently, the integrals can be evaluated by Gaussian Quadrature.

For body panels, the integrands of Eqs. (3) and (7) are regular for ordinary and large values of the compressible distance R, but they appear to be singular when R approaches to zero on the body surface. The latter leads to the occurrence of a number of singular-like integrals which requires special attention. For convenience of evaluation, two asymptotic cases for large and small parameters of νR are considered, namely the cases of $\nu R < 1$ and $\nu R > 1$, which are described in Ref. 30.

Boundary Conditions

It has been known for some time that an apex singularity for bodies exists in a wind-fixed system for an unsteady potential-flow formulation.

This apex singularity, along with the body-slope singularity, actually stems from the formal Taylor expansion of the unsteady velocities about the mean-body position for the boundary condition. Consequently, the wind-fixed unsteady boundary condition yields several second-order singular terms, all associated with h_B, such as ϕ_{oxt} and ϕ_{orr}.[16] In a more general derivation, the NLR group obtained a term $(\nabla S\cdot\nabla)\nabla\phi_0$ in the boundary condition which is indeed singular.[7] It appears that no clear resolution was stated in Refs. 7, 8, and 11 as to the remedy of the singular terms.

To circumvent such a type of singularity in a formulation for an oscillating body in either subsonic or supersonic flow has been a formidable task. Notably, Hoffman and Platzer[16] first pointed out such singularity appears only in the body-thickness terms in the series-expansion solution. But in the case of a slender body solution, they showed that the associated unsteady pressure coefficient is regular.

In an extensive analysis, Garcia-Fogeda and Liu[17] suggested an approach to adopt an approximate body-fixed formulation, which ignores the steady flow and mode shape interaction. This approach could totally circumvent the singularity problem. It has been further ascertained and adopted by many subsequent works in the unsteady treatments of bodies and wing-body combinations in supersonic, subsonic, and incompressible flows, e.g., Refs. 17–20.

Following Garcia-Fogeda and Liu[17] for an arbitrary elastic body performing oscillatory motion with given modes, the boundary condition in a body-fixed system reads[17]

$$V_0\cdot n = -(U_\infty\cdot n) \tag{8}$$

$$V_B\cdot n = F_B(n, V_0, h_B^{(n)}; k, M, \tau) \tag{9}$$

on the body surface $S_B(x, y, z) = 0$.

The boundary condition for the wing is the usual downwash conditions for lifting surface, i.e.

$$V_W\cdot n = F_W(h_W^{(n)}; k) \tag{10}$$

on the mean surface $S_W = 0$, where $F_W = h_W' + ikh_W$.

It is remarked that the body boundary conditions Eq. (9) include the influence of V_0, and therefore, τ and M. By contrast, the wing boundary conditions completely decouples from these parameters. It should be remarked that in the slender body limit, as τ approaches zero, Eq. (9) would not reduce to Eq. (10).

Pressure Coefficients and Generalized Forces

Based on our previous work,[12,17,19] the total pressure coefficient expressed in the body-fixed coordinate reads

$$\bar{C}_p = C_{p_0} + \delta_0 e^{ikt} C_p \tag{11}$$

and, the generalized forces can be expressed in terms of the mode functions h_{B_i} and h_{W_i} and the pressure coefficient

$$Q_{IJ} = \sum_{i=1}^{NB} C_{p_i}^{(J)} A_i (n_x h_B'^{(I)} z_0 - h_B^{(I)} n_z)_i + \sum_{i=1}^{NW} C_{p_i}^{(J)} A_i h_{W_i}^{(I)} \tag{12}$$

where $C_{p_i}^{(J)}$ is the pressure coefficient of the ith panel due to the Jth mode.

Body Wake Effect

The wake generated by flow separation at the tail section or behind the base of a body has considerable influence to the wing-body or body-alone aerodynamics. Previous methods[21–23] to model the body-wake flow have been ineffective and restrictive in their applications. These approaches usually require tedious iteration procedures and assumed initial wake shapes. In Ref. 22, the resulting wake solution could not assure the constant pressure conditions with an ending stagnation point at the wake closure. In addition, these methods are all confined to the treatment of steady or quasisteady incompressible flows.

As a new approach to the problem, the present wake model requires the following assumed conditions:

1) Base pressure C_{pB} must be given, a priori; therefore, the pressure of the adjacent panels to the body base is given by $\bar{C}_p = C_{pB}$.

2) No knowledge of the wake shape needs to be assumed initially.

3) Wake closure and its ending stagnation point can be assured (and verified numerically).

Based on these conditions imbedded singularities are placed in the proximity of the base regime to simulate the exterior wake flow. For steady flow the imbedded singularity is a source, whereas, for unsteady flow it is a doublet. Next, the constant pressure condition is imposed at the body base. When

this boundary condition is expressed in terms of Eq. (11), one obtains

$$C_{p_0} = C_{p_B} \tag{13}$$

$$C_p = 0 \quad \text{at the body base} \quad S(x = L, y, z) = 0 \tag{14}$$

Equation (17) can be combined with the expression of C_{p_0} and C_p of Eq. (11) to yield a compact expression in terms of the velocities, the mode shape and its derivatives, i.e.

$$A\phi = B\phi_0 \tag{15}$$

where A and B are both scalar operators

$$\begin{aligned} A &= \boldsymbol{V}_0 \cdot \nabla + ik \\ B &= \frac{d\boldsymbol{G}}{dx} \cdot \nabla + ik\boldsymbol{G} \cdot \nabla \\ \boldsymbol{G} &= \boldsymbol{G}(zh_B', 0, -h_B) \end{aligned} \tag{16}$$

The steady and unsteady body potentials now read

$$\begin{aligned} \phi_0 &= [-(1/4\pi)]I_B[(\sigma_{0i} + \sigma_s) \cdot H_i(\nu = 0)] \\ \phi &= [-(1/4\pi)]I_B[(\sigma_i + \mu_d) \cdot H_i(\nu) \cdot e^{-i\nu M\xi}] \end{aligned} \tag{17}$$

The location of the imbedded source σ_s and the imbedded doublet μ_d are placed along the extended body axis at $x = L + q_s$ and $x = L + q_d$, respectively, in the wake region near the base. The values of q_s and q_d are, in general, related to the wake length which is yet to be solved as part of the solution, ordinarily to be solved through an iteration procedure. However, our experience showed that empirical guidelines can be set up in which q_s can be confined to a width of $0.2–0.4L$, and q_d of $0.05–0.15L$ for any circular blunt base. By numerical experiment, it is found that the converged solutions are found to be rather insensitive to the precise location q_s and q_d (obtained by the iteration procedure) so long as they are placed within the width given.

In addition to the tangency conditions Eqs. (8) and (9), Eq. (15) is to be applied on the trailing-edge panels next to the base.

Thus, in contrast to the previous methods, the present body/wake solution method is simple, direct, and requires no iteration. The wake shape and pressure on the body are obtained simultaneously. Also, for all cases considered (seven bodies, that will be reported elsewhere), it was numerically verified that wake closure and the wake termination at a stagnation point are obtained.

Generalized Normal-Velocity Influence Coefficient (NIC)

Once the downwashes (the mode shape and the mean flow properties) on the RHS of Eqs. (8) and (9) are known, the unsteady source and doublet strengths for a given wing-body configuration can be solved along the surface according to the following NIC matrix equation:

$$\begin{bmatrix} \left(\frac{\partial\phi}{\partial n}\right)_{BB} & \left(\frac{\partial\phi}{\partial n}\right)_{BW} & \left(\frac{\partial\phi}{\partial n}\right)_{B\text{-Wake}} \\ \left(\frac{\partial\phi}{\partial n}\right)_{WB} & \left(\frac{\partial\phi}{\partial n}\right)_{WW} & \left(\frac{\partial\phi}{\partial n}\right)_{W\text{-Wake}} \\ (A\phi)_{\text{Wake-}B} & (A\phi)_{\text{Wake-}W} & (A\phi)_{\text{Wake-Wake}} \end{bmatrix} \begin{Bmatrix} \sigma \\ \Delta C_p \\ \mu \end{Bmatrix} = \begin{Bmatrix} F_B \\ F_W \\ B\phi_0 \end{Bmatrix} \tag{18}$$

where the element $(\partial\phi/\partial n)_{WB}$ represents the NIC induced on the wing by the body, $(\partial\phi/\partial n)_{\text{Wake-}W}$ the NIC induced on the wake by the wing, the wake element $(A\phi)_{B\text{-Wake}}$ the NIC induced on the body by the wake, etc., and μ = the unknown imbedded singularity strength, σ_s or μ_d. Once the unknowns σ, ΔC_p, and μ are solved from Eq. (18), the unsteady potential ϕ and velocities u, v, and w can be obtained from Eqs. (1), (6), and (7).

Table 1 Generalized aerodynamic force coefficient for AGARD wing horizontal-tail combination in antisymmetric motion with tail above wing at $z = 0.6$

$k = 0.01$ and 1.50, and $M = 0.8$

Mode no.	Mode
1	Wing twist $f = y(x - 2.25\|y\| - 0.85)$
2	Wing bending $f = y\|y\|$
3	Tail roll $f = y$
4	Tail pitch $f = \text{sgn}(y)(x - 3.35)$

$$\bar{Q}_{ij} = -\frac{1}{2} Q_{ij} \qquad \bar{Q}_{ij} = -\frac{1}{2}\int_A \int C_{pi} f_j \, dA = Re(\bar{Q}_{ij}) + ik\, Im(\bar{Q}_{ij})$$

Pressure mode i / Deflection mode j (i, j)	$Re(\bar{Q}_{ij})$, $k = 0.01$		$Im(\bar{Q}_{ij})$, $k = 0.01$		$Re(\bar{Q}_{ij})$, $k = 1.5$		$Im(\bar{Q}_{ij})$, $k = 1.5$	
	Present	DLM	Present	DLM	Present	DLM	Present	DLM
1,1	−0.0645	−0.0733	0.1772	0.1635	−0.1634	−0.1644	0.1951	0.1782
2,1	0.2870	0.2776	0.3853	0.3788	0.2248	0.2243	0.4112	0.3974
3,1	−0.0685	−0.0660	0.0386	0.0347	−0.0347	−0.0343	0.0452	0.0432
4,1	−0.0758	−0.0718	0.0416	0.0371	−0.0429	−0.0406	0.0522	0.0492
1,2	−0.0000	0.0000	−0.0385	−0.0440	−0.1407	−0.1232	−0.0319	−0.0387
2,2	−0.0000	0.0000	0.2068	0.1961	−0.3355	−0.3303	0.2268	0.2147
3,2	−0.0000	0.0000	−0.0447	−0.0420	−0.0514	−0.0496	0.0068	0.0052
4,2	−0.0000	0.0000	−0.0497	−0.0459	−0.0607	−0.0573	0.0066	0.0051
1,3	0.0000	0.0000	0.0000	−0.0000	−0.0008	−0.0008	−0.0004	−0.0004
2,3	0.0000	0.0000	0.0002	0.0002	−0.0015	−0.0015	−0.0005	−0.0006
3,3	−0.0000	0.0000	0.4082	0.3949	−0.2932	−0.2914	0.4497	0.4322
4,3	−0.0000	0.0000	0.4583	0.4355	−0.5246	−0.5089	0.5257	0.4945
1,4	−0.0001	−0.0001	−0.0000	0.0001	−0.0027	−0.0028	−0.0002	−0.0001
2,4	0.0002	0.0002	−0.0009	−0.0011	−0.0045	−0.0046	0.0007	0.0007
3,4	0.6806	0.6775	0.9991	0.9986	0.3477	0.3278	1.0915	1.0701
4,4	0.7396	0.7205	1.5006	1.4769	−0.0186	−0.0264	1.6722	1.6094

Results and Discussion

Nonplanar AGARD Wing-Tail

Generalized force $\bar{Q}_{11}$ (lift coefficient) due to a nonplanar AGARD wing-tail configuration under heaving motion at $M = 0.8$ and $k = 1.5$ vs the tail height z/s (s being the semispan), is shown in Fig. 1. In the overall range of z/s, it is seen that the present results are in good agreement with those of DLM and of piecewise continuous kernel function method (PCKFM).[24]

For the nearly-coplanar case, where the present can be tested in the asymptotic limit of small z, the computed results are in better agreement with that of PCKFM. However, it should be noted that the present formulation adopts a similar approach to that in Ref. 1 for the analytical treatment of the nearly-coplanar limit.

Table 1 presents the generalized aerodynamic force coefficients for the same coplanar AGARD configuration in four antisymmetric modes of motion; 1) a wing twist mode, 2) a wing bending mode, 3) a tail rolling mode, and 4) a tail pitching mode at $M = 0.8$ and $k = 0.01$ and 1.5. Comparisons with DLM results for all values of $\bar{Q}_{ij}$ (in Ref. 1) show overall agreement. Note that $\bar{Q}_{ij} = -\frac{1}{2}Q_{IJ}$ of Eq. (12) up to 9% difference in values are found for some coefficients. It is believed that such discrepancies are attributed mostly to different orders of doublet distribution used in both methods but not in the kernel function evaluation.

LMSC Blunt Body

Figure 2 compares the present results with the experimental pressure distributions along the Lockheed Missile and Space Company (LMSC) blunt-based body in an incompressible flow. The experimental data is given by Rattayya et al.[23] Notice that the forebody has two slope discontinuities. It is seen that the present (no wake) result begins to deviate from the measured data at a forebody portion of $0.3L$, where the second slope discontinuity is located. The C_{p0} result gradually deteriorates towards the body base and the pressure approaches the freestream pressure p_∞ as an asymptote. This is clear as can be seen from the no-wake surface panel method (SPM), or from the unified subsonic and supersonic aerodynamics (USSAERO)[15] formulation, the perturbed velocities immediately beyond the base panels would vanish, thus rendering the local pressure there approaching that of freestream. By contrast, the present (with wake) result shows remarkably close agreement with measured data, which indicates that once the base pressure is properly specified, the wake-model formulation results in a correct pressure distribution which is uniformly valid throughout the body length.

Figure 3 shows the side views of the computed base-flow of the LMSC body, according to the present SPM (no wake) and the present SPM (with wake). The direction and the length of the arrows indicate the flow direction and the velocity magnitude, respectively. As expected, the no-wake flowfield velocities appear to be nearly uniform showing their immediate return to the freestream condition. It can be seen that the present wake model appears to closely simulate the outer wake flow. The dashed line is indeed the dividing streamline which defines the wake closure, or the computed wake shape. It is clearly shown that the stagnation point at the end of the wake is automatically captured by the present calculation. The computed wake flow is only physically meaningful in the outside wake flow region, whereas, the computed flow inside the wake is of no physical significance.

NASA Blunt Cone

Figure 4 shows the effect of Mach number on the stability of a blunt-cone at a pitching-axis location, $X_G = 0.73$. The experimental data for this body has been obtained by William and Wehrend.[25]

For the case without wake, both the static and damping moment predicts reasonably well with the overall trend of the measured data. When the wake is taken into account, it is

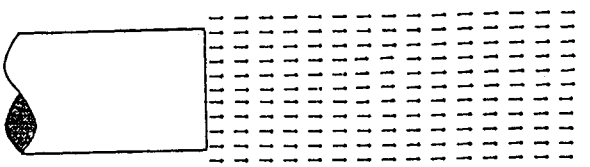

a) Without wake model

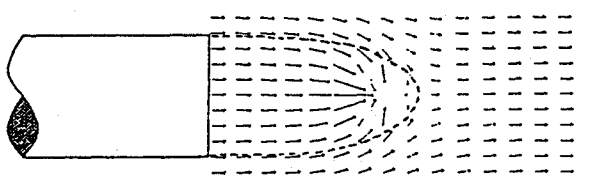

b) With wake model

Fig. 3 Computed wake shape for a LMSC blunt body at $M = 0$ and $\alpha = 0$ deg; a Meridian-Plane view.

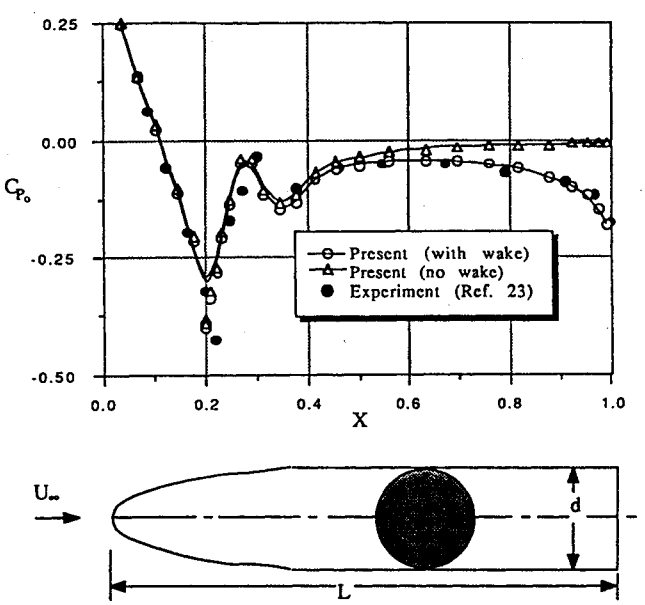

Fig. 2 Comparison of surface pressure distribution for a LMSC blunt body ($L/d = 5$) at $\alpha = 0$ deg, $M = 0$ and base pressure $C_{pb} = -0.169$.

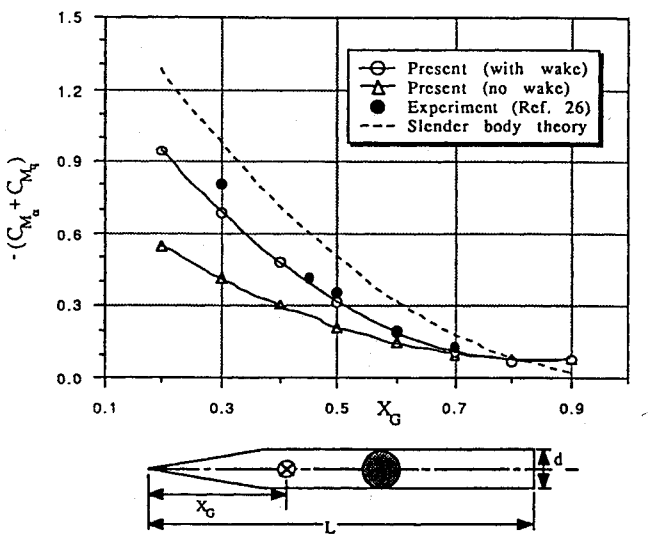

Fig. 4 Effect of the pitching axis location on damping-in-pitch moment for a cone-cylinder body ($L/d = 7.5$) at $M = 0.3$.

seen that it improves substantially on the static moment throughout the Mach number range considered.

Since no transition effect or boundary-layer effect was taken into account in the present calculation, the improved agreement between the measured static moment and the present results clearly indicate that the wake effect is of primary importance for the prediction of stability derivatives, an effect totally ignored in almost all previous analysis. The present wake model has less impact on the damping derivative. It is believed that the present base-flow boundary condition is basically quasisteady, which may be overly imposed on the unsteady pressure ($C_P = 0$). Efforts to improve the base-pressure boundary condition are currently underway.

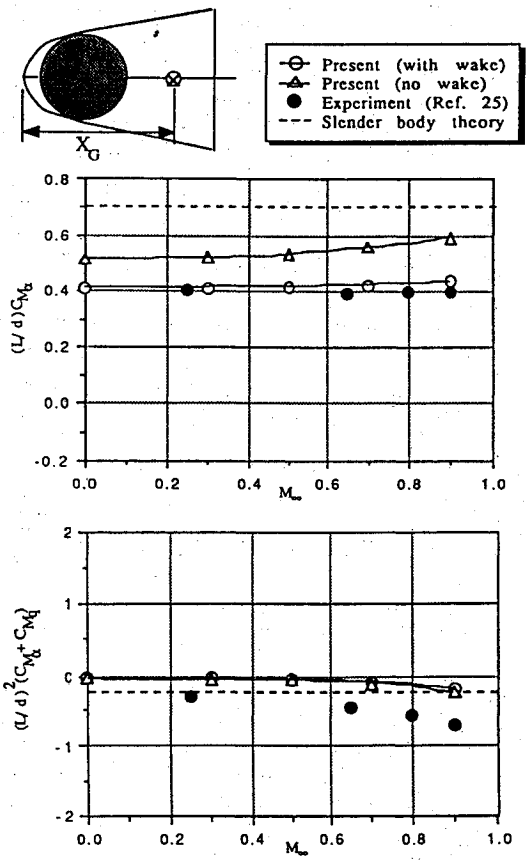

Fig. 5 Effect of Mach number on moment derivatives for a NACA blunt cone ($L/d = 1.2$) with pitching axis at $X_G = 0.73$.

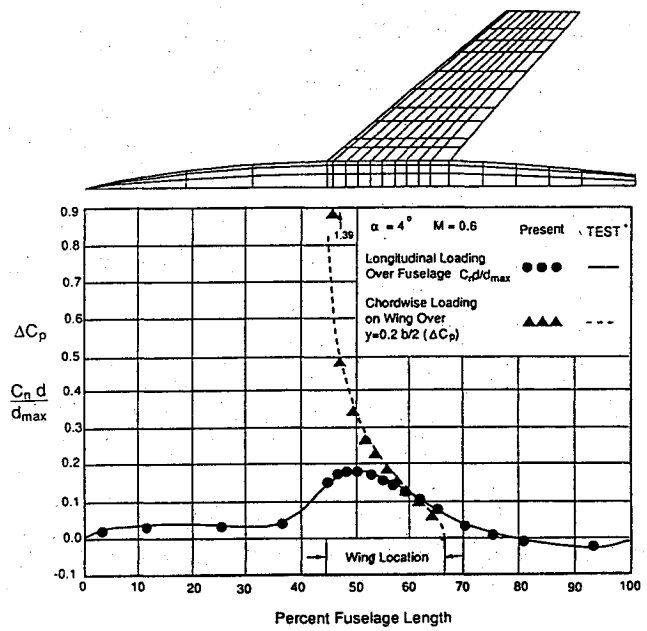

Fig. 6 Static loading of a NACA wing-body configuration; $M = 0.6$ and $\alpha = 4$ deg.

Damping Moment of a Cone-Cylinder

Figure 5 shows the effect of the pitching axis location X_G on the aerodynamic damping moment for a slender cone-cylinder of $L/d = 7.5$ at a Mach number equal to 0.3. The experimental data are given by Bykov.[26]

It is seen that the present result (with wake but without considering the boundary layer effect) is in good agreement with Bykov's measured damping moment. Notice that the wake effect is to increase the negative damping of the body. As expected, all methods confirm that negative damping can be increased as the pitching axis moves toward the apex. However, in terms of damping moments for flight dynamics and design applications, it is important to note that the slen-

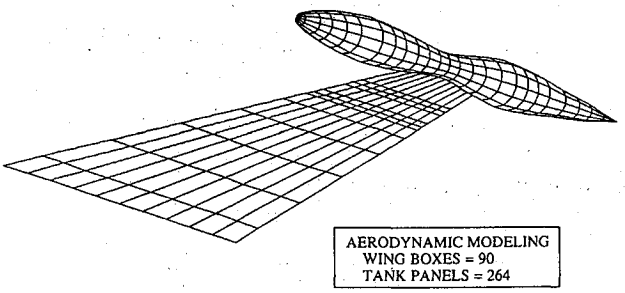

Fig. 7 NLR wing-tip-tank configuration showing paneling scheme.

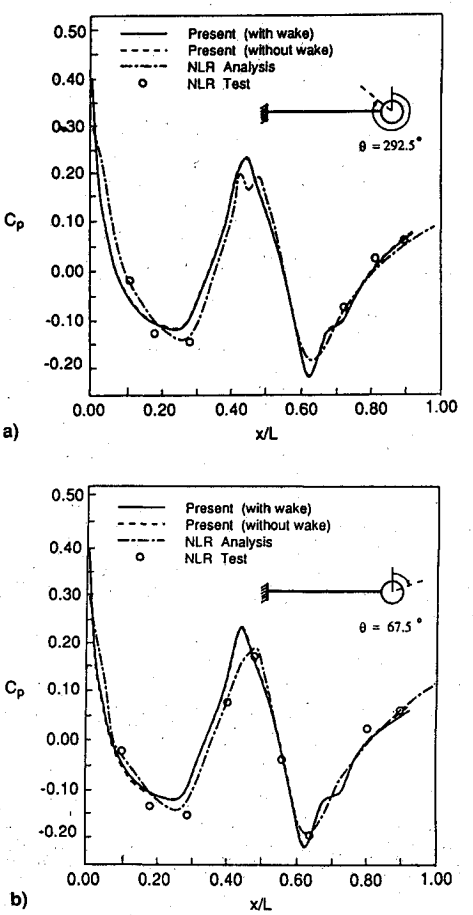

Fig. 8 Steady pressure distribution along the tip-tank of NLR wing-tip-tank configuration; $M = 0.45$, $\alpha = 0$ deg: a) $\theta = 292.5$ deg and b) $\theta = 67.5$ deg.

der-body-theory prediction is most unconservative, whereas, the present (no wake) prediction is most conservative.

NACA Wing-Body Interference

Longitudinal loading (c_{nd}/d_{max}) over a 10% thick body with a taper wing (AR = 4.0 and tapered ratio = 0.6) are presented in Fig. 6. The measured data have been obtained by Loving and Eastbrooks.[27]

The sectional normal force pressure coefficient C_n is defined as

$$C_n = \frac{1}{d}\int_0^{2\pi} C_p \, d\theta \tag{19}$$

where d and d_{max} represents the diameter and maximum diameter of the body, respectively.

A bump-like loading along 40–70% of the body length is observed as a result of the wing-body interference due to the presence of the tapered wing. In addition, lifting pressure distribution along the wing chord is also plotted at 20% semispanwise location. It is seen that good agreement is found between the computed and measured results. Thus, the steady aerodynamic option of the present method is validated by the present interference example.

In what follows, calculations based on two sets of NLR measurements were performed (Refs. 8 and 10) involving the model configurations shown in Ref. 10. The model paneling schemes of these two cases are shown in Figs. 7 and 11. Here, all forces definitions such as normal load C_z and side load C_y strictly follow that of NLR. For discussion of these NLR configurations, Table 2 is provided to relate the present figure sequence to those in the NLR publications.

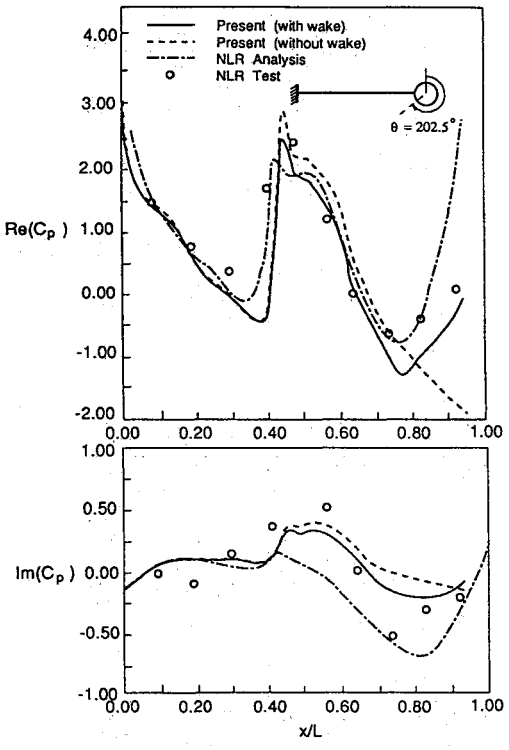

Fig. 9 Unsteady pressure distribution along the tip-tank of NLR wing-tip-tank configuration; M = 0.45, α = 0 deg, k = 0.305, $\bar{x}_0$ = 0.15c_R, and θ = 202.5 deg.

NLR Wing Tip-Tank Configuration

Based on the configuration and the paneling scheme shown in Fig. 7, the computed steady pressure coefficients along the tip-tank at two azimuthal angles, 1) θ = 292.5 deg and 2) θ = 67.5 deg, are presented in Fig. 8. The present results with or without wake appear to be in good agreement with each other and with NLR's computed and measured data.

However, no "leading-edge peak" due to the wing leading edge as claimed by NLR was obtained in the present result. It should be mentioned that the wake model was set up by simply imposing the base pressure C_{p_B} to match the measured

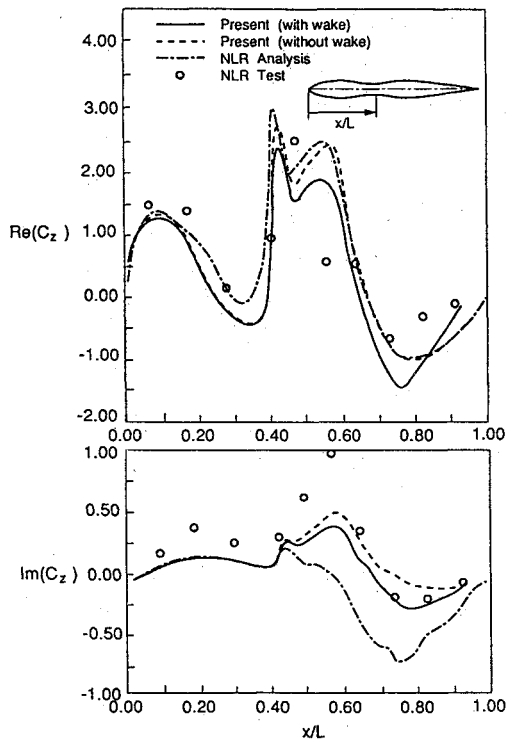

Fig. 10 Unsteady normal load distribution along the tip-tank of NLR wing-tip-tank configuration; M = 0.45, α = 0 deg, k = 0.305, and $\bar{x}_0$ = 0.15c_R.

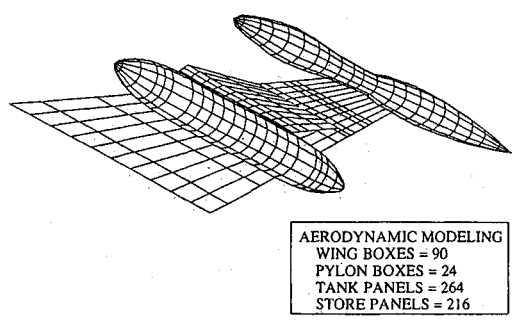

Fig. 11 NLR wing-tip-tank-pylon-store configuration showing paneling scheme.

Table 2 Cases of comparison with NLR

Present Fig. no.	8	9 and 10	12	13	14 and 15	17
NLR Fig. no.	5 and 6	5 and 6	13	9 and 10	11 and 12	9b and 15
Ref. no.	7	8	9	8	8	28

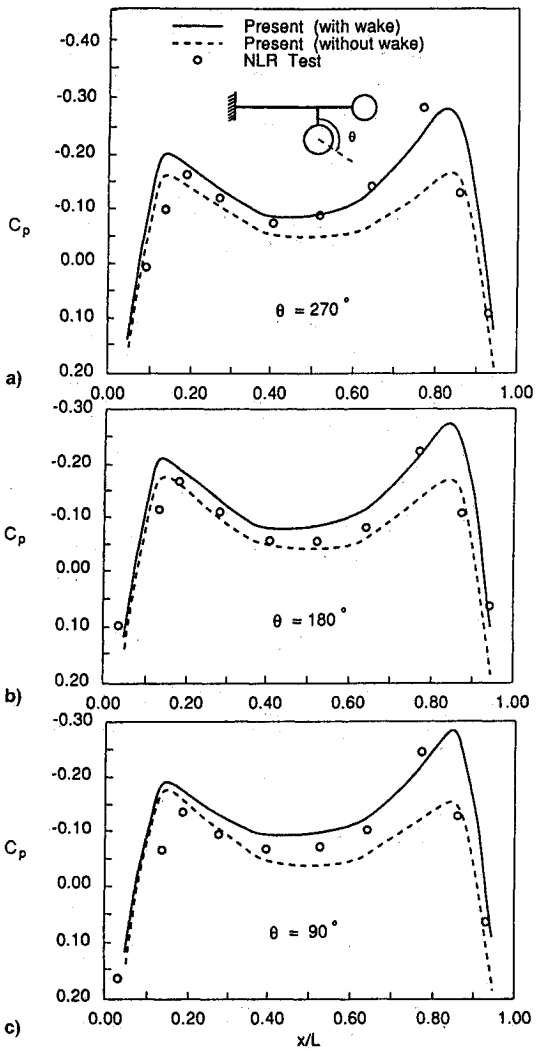

Fig. 12 Steady pressure distributions along the store of NLR wing-tip-tank-pylon store configuration; $M = 0.45$, $\alpha = 0$ deg: a) $\theta = 90$ deg, b) $\theta = 180$ deg, and c) $\theta = 270$ deg.

C_p at $X/L = 0.9$. It is seen that solutions with and without wakes are almost indistinguishable. Here the wake option could be used to verify the flow situation at the body tail. With a selected C_{pB} input, if the solution with wake appears to be the same as that without wake, the program logic would determine that no flow separation occurs, which is the present case.

Figure 9 presents the unsteady pressures along tip-tank at an azimuthal angle $\theta = 202.5$ deg. It is seen that the present results are in good agreement with the NLR measured data. This time, the leading-edge peaks are obtained by the present computation. The present no-wake in-phase C_P appears to deteriorate towards the tail of the tip-tank, whereas, that with wake appears to correlate best with the measured data. This is expected, because the flow is known to separate at the rear in this case, according to Ref. 8. For the out-of-phase C_P, the NLR computed results show a discrepancy with the measured data starting from the midbody.

Figure 10 presents the unsteady normal load C_z along the tip-tank. It is seen that the present predicted values of the in-phase and out-of-phase C_z are in better agreement with the measured data than those of NLR, particularly for the cases with the wake model. In addition, the NLR's out-of-phase result show considerable departure from the measured data. The discrepancies found for the NLR's computed results in Figs. 9 and 10 could be due to a number of causes, which could amount to any combination of the three issues considered presently (see Introduction).

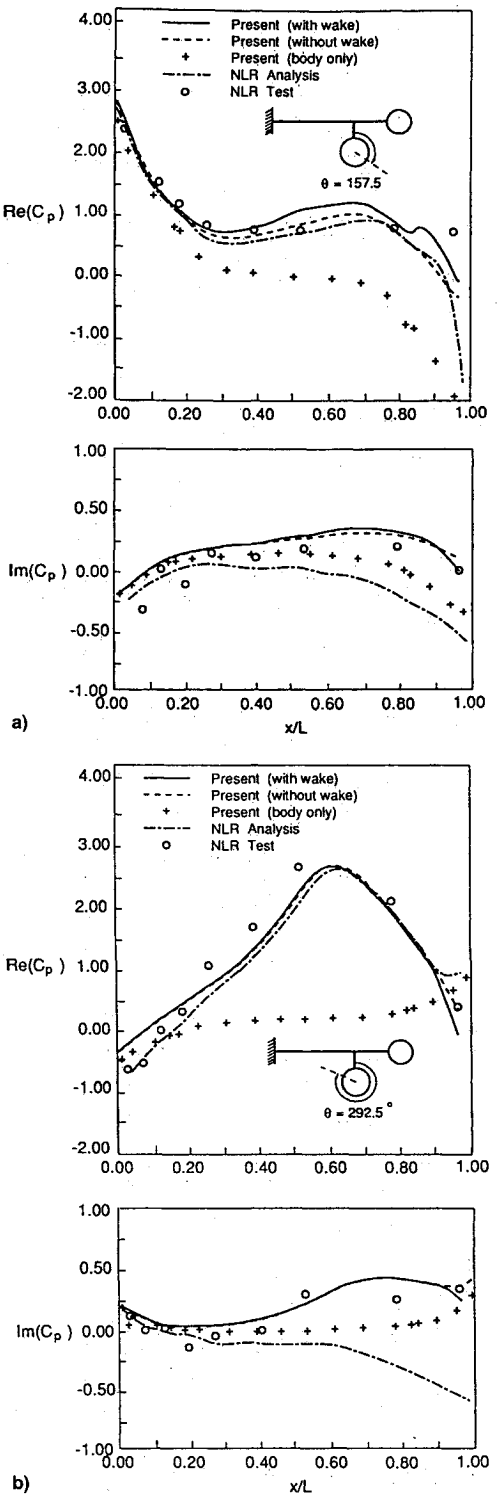

Fig. 13 Unsteady pressure distributions along the store of NLR wing-tip-tank-pylon store configuration at a) $\theta = 157.5$ deg and b) $\theta = 292.5$ deg. $M = 0.45$, $\alpha = 0$ deg, $k = 0.305$, and $\bar{x}_0 = 0.15c_R$.

NLR Wing-Tip-Tank-Pylon Store

The computed steady pressure distributions along the store at three azimuthal angles, namely, $\theta = 90$, 180, and 270 deg, are presented in Fig. 12. The solution with wake is seen to have better agreement with the measured data than that without a wake. This leads one to believe that the flow might have separated at the body tail in this experiment, although no such information was supplied in Ref. 10.

Figure 13 presents the unsteady pressure distributions along the store at two azimuthal angles: 1) $\theta = 157.5$ and 2) $\theta = 292.5$ deg. From the present computed results, it is seen that

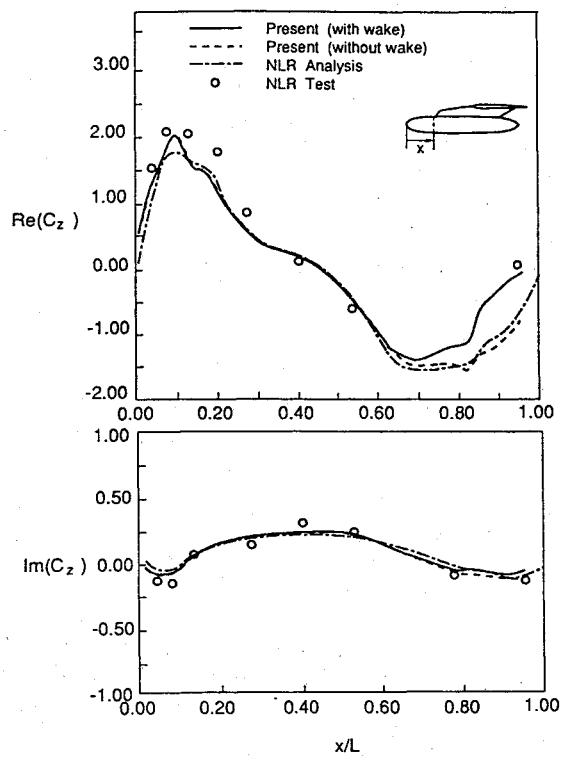

Fig. 14 Unsteady normal load distribution along the store of NLR wing-tip-tank-pylon store configuration; $M = 0.45$, $\alpha = 0$ deg, $k = 0.305$, and $x_0 = 0.15c_R$.

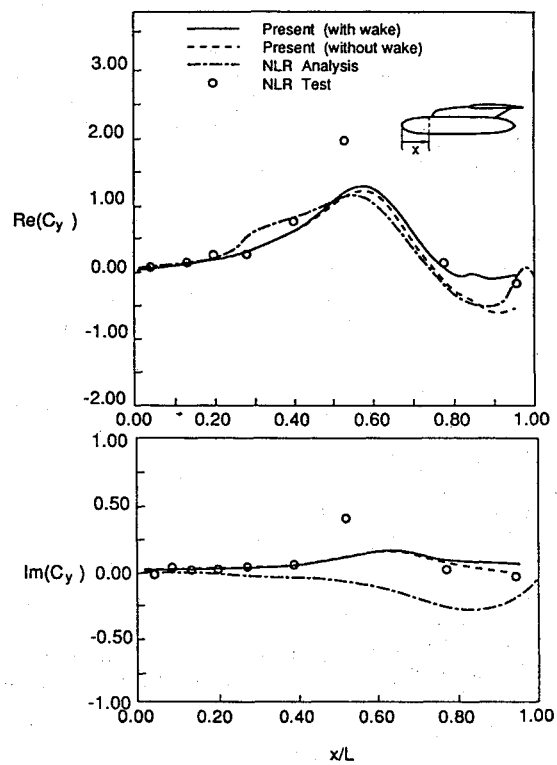

Fig. 15 Unsteady side load distribution along the store of NLR wing-tip-tank-pylon store configuration; $M = 0.45$, $\alpha = 0$ deg, $k = 0.305$, and $\bar{x}_0 = 0.15c_R$.

adding the wing-tip-tank-pylon has altered the unsteady pressure distributions on the store substantially. The same observation was pointed out in Ref. 8. In all cases, the present results with or without wake are in good agreement with the measured data. In particular, the solution with wake seems to show better agreement than the no-wake solution for the in-phase C_P, and there the solution also shows a trailing-edge peak due to pylon-store interaction (at $\theta = 292.5$ deg).

On the other hand, NLR's computed results in the out-of-phase C_P indicates a solution departure from the measured data starting from the midbody section, and further deteriorates towards the body tail. Again this discrepancy could be caused by the insufficiency in the NLR method in treatments of wing-body interference, as well as the boundary condition employed. By contrast, it is seen that both present solutions results in much better agreement with the measured data, especially near the body tail.

Figures 14 and 15 present the unsteady normal forces and unsteady side forces along the store, respectively. It is seen that the present solution with wake is in better agreement with the measured data than others considered. Careful observation of the measured data of Figs. 13–15 reveals that the unsteady pressures and force coefficients tend to approach zero at the body tail. Presumably, if the flow-separation at the tail can be justified from the study in Fig. 12, then the present finding should support the present wake model [Eq. (14)] being physically plausible for a close-ended body as well.

At least for bodies in mildly unsteady motions, the current wake model is further validated by its consistent agreement with these measured data which were obtained in the low-frequency range ($k = 0.305$).

F-5 Wing with Tip Missile

In Fig. 16, another NLR test configuration, involving a F-5 wing tip missile, is modeled by 72 panels for the wing, 14 panels for the pylon, 16 panels for the four canard fins, 24 panels for the four aft fins, and 112 body panels for the missile

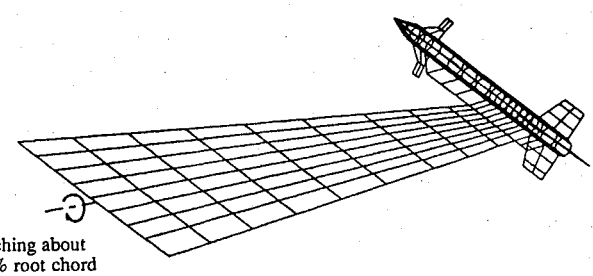

Fig. 16 Northrop F-5 wing with tip missile configuration showing paneling scheme.

body. This configuration was wind-tunnel tested by a NLR group led by Tijdeman.[28]

Figure 17 presents the computed spanwise normal load distribution and the computed pitching moment distribution for the clean wing, and the complete configuration with pitching axis located at 50% root chord at $M = 0.6$ and $k = 0.2$. The measured trend for the in-phase normal force shows a departure course between the clean-wing results and that of the complete configurations starting from the root chord, and the difference widens up towards the wing ip. Both the present method and the NLR method confirm the same trend. However, the present results correlate closer to the measured data than the NLR results.

One recalls the counterpart study of the same configuration in Ref. 12 for unsteady supersonic flow (Fig. 21,[12] $M = 1.35$ and $k = 0.1$). Judging from the predicted (and measured) damping forces and moments of the same complete configuration (and the clean wing), it can be concluded that the configuration is dynamically unstable in subsonic flow ($M = 0.6$), whereas, it is marginally stable in supersonic flow ($M = 1.35$). In general, the tip-missile effect on the wing appears to have a more pronounced impact on the in-phase forces and moments than the out-of-phase ones.

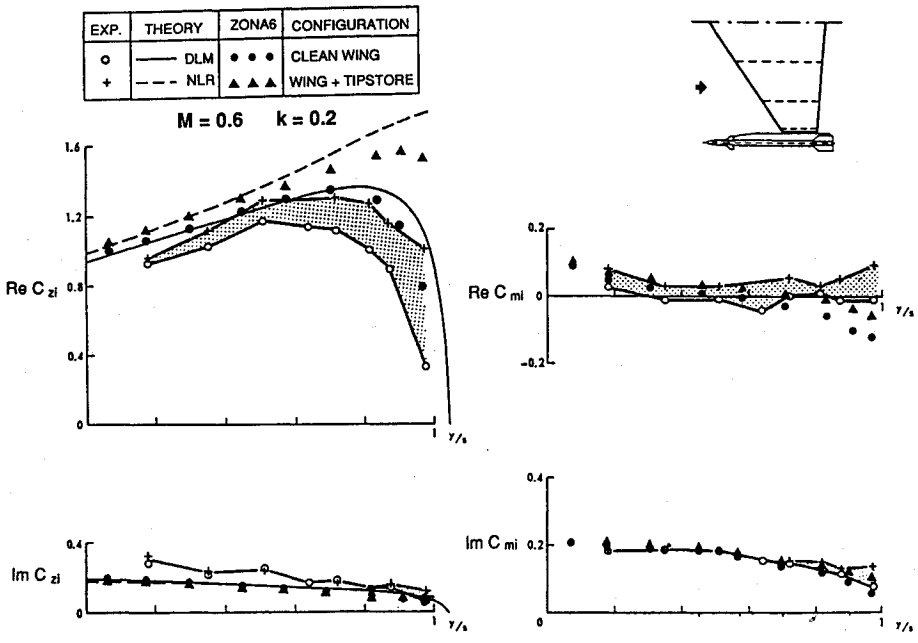

Fig. 17 Unsteady spanwise normal forces and pitching moment for the clean F-5 wing and the complet wing with tip missile configuration at $M = 0.6$, $k = 0.2$ and $\bar{x}_0 = 0.5\ C_R$.

Conclusions

A general unsteady subsonic method has been developed for computation of wing-body aerodynamics including the body-wake effect. For aeroelastic applications, the wing-body configuration could be modeled to represent realistic aircraft with various combinations of external stores. As a counterpart of our unsteady supersonic method for the wing-body (the HGM, or the ZONA51[29] and the ZONA7[12] series), the present subsonic development is considered an advancement over the previous methods in the following sense:

1) Correct unsteady boundary condition is applied on the body surface.

2) Body/wake effect is properly accounted for by introducing a new imbedded singularity wake model. Such an effect is found to substantially influence the pressures and the stability derivatives for the bodies and wing-store configuration.

3) Wing-body influence can be more accurately assessed by the present panel method for lifting surfaces which is one order higher than that of DLM.

For code verification, computed results of various lifting surfaces, bodies, and a number of wing-store combinations are compared with existing computed and measured data. It can be seen from all cases presented that the present results, with or without the wake model, consistently shows best agreement with the measured data among existing methods.

Furthermore, a comparative study with results obtained from a previous supersonic investigation (computed by ZONA7[12]) on the F-5 Wing with tip missile and those present in Fig. 16 was conducted. The computed results confirms those measured by NLR that 1) the wing-body interference effect is more pronounced in subsonic flow; and 2) the configuration is less dynamically stable in subsonic flow. Therefore, the present case, along with others considered, warrants a more active unsteady subsonic method for aeroelastic analysis.

Meanwhile, a computer program (code name ZONA6) has been developed for aeroelastic application to realistic aircraft configurations. This program contains several salient features: 1) it has a built-in subsystem for input; 2) it is valid for all reduced frequencies; and 3) it is applicable to complex elastic wing-body combinations with any given mode. Therefore, we believe that an accurate, versatile, and effective unsteady subsonic method is finally at hand for aeroelastic applications.

Acknowledgment

The authors would like to thank Z. X. Yao of Arizona State University for valuable suggestions and discussion. In particular, they wish to thank Professor R. M. C. So of Arizona State University for suggesting the wake model which is instrumental for the present development. Thanks are also due to L. E. Ericsson of LMSC and M. F. Platzer of the Naval Postgraduate School for helpful discussion and providing the supporting references.

References

[1]Rodden, W. P., Giesing, J. P., and Kalman, T. P., "New Method for Nonplanar Configurations," *AGARD Conference Proceedings*, CP-80-71, Pt. II, No. 4, 1971.

[2]Giesing, J. P., Kalman, T. P., and Rodden, W. P., "Subsonic Steady and Oscillatory Aerodynamics for Multiple Interfering Wings and Bodies," *Journal of Aircraft*, Vol. 9, No. 10, 1972, pp. 693–702.

[3]Morino, L., "A General Theory of Unsteady Compressible Potential Aerodynamics," NASA CR 2464, 1974.

[4]Johnston, F. T., and Rubbert, P. E., "Advanced Panel Type Influence Coefficient Methods Applied to Subsonic Flows," AIAA Paper 75-50, Jan. 1975.

[5]Bristow, D. R., and Hawk, J. D., "Subsonic Panel Method for Designing Wing Surfaces from Pressure Distribution," NASA CR 3713, July 1983.

[6]Coppersmith, R. M., Youngren, H. H., and Bouchard, E. E., "Quadrilateral Element Panel Method (QUADPAN)," Theoretical Rept. (Version 3), Lockheed-California Co., LR 30400, Burbank, CA, July 1983.

[7]Bennekers, B., Roos, R., and Zwaan, R. J., "Calcon of Aerodynamic Loads on Oscillating Wing/Store Combinations in Subsonic Flow," AGARD Specialists Meeting on Wing-with-Stores Flutter, CP-162, Paper 4, Munich, Germany, 1974.

[8]Roos, R., Bennekers, B., and Zwaan, R. L., "A Calculation Method for Unsteady Subsonic Flow About Harmonically Oscillating Wing-Body Configurations," *Journal of Aircraft*, Vol. 14, No. 5, 1977, pp. 447–454.

[9]Hounjet, M. H. L., "Calculation of Unsteady Subsonic and Supersonic Flow About Oscillating Wings and Bodies by a New Panel Method," *Proceedings of the European Forum on Aeroelasticity and Structural Dynamics*, DGLR/NLR/RAe&/ONERA, Aachen, Germany, April 1989.

[10]Renirie, L. T., "Analysis of Measured Aerodynamic Loads on an Oscillating Wing-Store Combination in Subsonic Flow," AGARD Specialists Meeting on Wing-with Stores Flutter, CP-162, Paper 5,

Munich, Germany, 1974.

[11]Labrujere, T. E., Roos, R., and Erkelens, L. J. J., "The Use of Panel Methods with a View to Problems in Aircraft Dynamics," National Aerospace Lab., MP-77009U, The Netherlands.

[12]Chen, P. C., and Liu, D. D., "Unsteady Supersonic Computations of Arbitrary Wing-Body Configurations Including External Stores," *Journal of Aircraft*, Vol. 27, No. 2, 1990, pp. 108–116.

[13]Laschka, B., "Der Harmonisch Schwingende Rechtekflugel bei Uberschallstromung," Ernst heinkel Flugzugbau, GmbH, Rept., 1960.

[14]Desmarais, R. M., "An Accurate and Efficient Method for Evaluating the Kernel of the Integral Equation Relating Pressure to Normal Wash in Unsteady Potential Flow," AIAA Paper 82-0687, 1982.

[15]Woodward, F. A., "Analysis and Design of Wing-Body Combination at Subsonic and Supersonic Speeds," *Journal of Aircraft*, Vol. 5, No. 6, 1968, pp. 53–59.

[16]Hoffman, G. H., and Platzer, M. F., "On Supersonic Flow Past Oscillating Bodies of Revolution," *AIAA Journal*, Vol. 4, No. 2, 1966, pp. 370, 371.

[17]Garcia-Fogeda, P., and Liu, D. D., "Analysis of Unsteady Aerodynamics for Elastic Bodies in Supersonic Flow," *Journal of Aircraft*, Vol. 24, No. 12, 1987, pp. 833–840.

[18]Garcia-Fogeda, P., and Liu, D. D., "Supersonic Aeroelastic Applications of Harmonic Potential Panel Method to Oscillating Flexible Bodies," *Journal of Spacecraft and Rockets*, Vol. 25, No. 4, 1988, pp. 271–277.

[19]Garcia-Fogeda, P., Chen, P. C., and Liu, D. C., "Unsteady Supersonic Flow Calculations for Wing-Body Combinations Using Harmonic Gradient Method," *AIAA Journal*, Vol. 28, No. 4, 1990, pp. 635–641.

[20]Wu, M. S., Garcia-Fogeda, P., and Liu, D. D., "Potential Flow over Bodies of Revolution in Unsteady Motions," *AIAA Journal*, Vol. 27, No. 6, 1989, pp. 725–733.

[21]Chou, Y. S., "Asymmetric Cavity Flows Past Slender Bodies of Revolution," *Journal of Hydronautics*, Vol. 8, No. 1, 1974, pp. 13–18.

[22]Struck, H. G., "Discontinuous Flows and Free Streamline Solutions for Axisymmetric Bodies at Zero and Small Angle of Attack," NASA TN D-1768, 1963.

[23]Rattayya, J. V., Brosseau, J. A., and Chisholm, M. A., "Potential Flow About Bodies of Revolution with Mixed Boundary Conditions-Cross Flow," *Journal of Hydronautics*, Vol. 15, Nos. 1–4, 1981, pp. 81–89.

[24]Lottati, I., and Nissim, E., "Nonplanar, Subsonic, Three-Dimensional Oscillatory Piecewise Continuous Kernel Function Method," *Journal of Aircraft*, Vol. 22, No. 12, 1985, pp. 1043–1048.

[25]William, R., and Wehrend, W. R., "An Experimental Evaluation of Aerodynamic Damping Moments of Cones with Different Centers of Rotations," NASA TN D-1768, 1963.

[26]Bykov, V. S., "Calculation of the Characteristics of Aerodynamic Damping of Bodies of Revolution," FTD-HT-23-1363-74, June 1974.

[27]Loving, D. L., and Eastbrooks, B. B., "Transonic-Wing Investigation in the Langley 8-Foot High-Speed Tunnel at High Subsonic Mach Numbers and a Mach Number of 1.2," NACA RM L51F01, Sept. 1951.

[28]Tijdeman, J., et al., "Transonic Wind-Tunnel Tests on an Oscillating Wing with External Stores: Part I-IV, the Wing with Tip Store," Air Force Flight Dynamics Lab., AFFDL-TR-78-194, Wright-Patterson AFB, OH, May 1979.

[29]Chen, P. C., and Liu, D. D., "A Harmonic Gradient Method for Unsteady Supersonic Flow Calculations," *Journal of Aircraft*, Vol. 22, No. 15, 1985, pp. 371–379.

[30]Liu, D. D., Lee, H. W., and Chen, P. C., "Unsteady Subsonic Aerodynamics for Bodies and Wings with External Stores Including Wake Effect," International Forum on Aeroelasticity and Structural Dynamics, Paper 91-060, DGLR/NLR/RAeS/ONERA Aachen, Germany, June 3–6, 1991.